Effect of Sodium on HCl Hydrate Diffusion in Ice: Evidence for Anion−Cation Trapping

Frank E. Livingston[†,‡] and Steven M. George*[,†,§]

Department of Chemistry and Biochemistry and Department of Chemical Engineering, University of Colorado, Boulder, Colorado 80309-0215

Received: December 13, 2001

The effects of sodium (Na) on hydrogen chloride (HCl) hydrate diffusion in ice were investigated using infrared laser resonant desorption depth-profiling (LRD) techniques. By exciting the O−H stretching vibration in H_2O, LRD was used to depth-profile into ice sandwich multilayers containing either an HCl or a Na/HCl interlayer. Diffusion coefficients for HCl were determined by measuring the relaxation of the HCl concentration gradient versus time. The HCl hydrate diffusion coefficient at 190 K in pure ice was $D = 5.1(\pm 1.7) \times 10^{-11}$ cm^2/s and lower for the Na/HCl interlayers. The HCl diffusion coefficients varied from $D = 1.2(\pm 0.5) \times 10^{-11}$ cm^2/s to $D \leq 9.0 \times 10^{-13}$ cm^2/s for initial interlayer molar ratios of Na/Cl = 0.04 to Na/Cl = 0.5, respectively. The effect of Na on HCl hydrate diffusion in ice is attributed to anion−cation trapping. Similar trapping interactions may influence the distribution of species in ice cores used to interpret the historical record of Earth's atmosphere.

I. Introduction

Ice is the most prevalent molecular solid on Earth and plays a special role in many global atmospheric and environmental processes.[1−3] The Greenland and Antarctic ice sheets contain 99% of the ice and 80% of the freshwater on Earth.[3] Trace gas phase and aerosol species can be irreversibly adsorbed onto ice surfaces and incorporated into the snowpack. Consequently, glacial and polar ice cores provide a history of Earth's atmosphere dating back over 420 000 years.[4] Ice core analysis yields signatures of local temperature fluctuations, geologic activity, and anthropogenic effects on the environment.[2,4,5]

To extract chronological records of Earth's atmosphere, the concentrations of species encapsulated in the ice core must be correlated with ambient atmospheric concentrations. The partitioning of species between the gas/aerosol and the solid ice phases is defined by the air-to-snow transfer function.[2,6,7] Postdepositional processes such as diffusion, desorption, and chemical or photochemical reactions can perturb the air-to-snow transfer function.[2,6,7] Postdepositional diffusion can smooth concentration profiles and hide seasonal trends of trace species contained in the ice. Diffusion can also be coupled with chemical interaction to either destroy the identity of a species or trap the species and limit further migration.

The solubility and diffusion of hydrogen chloride (HCl) in ice have received attention because HCl plays a role in controlling the acidity of the atmosphere.[8] The interaction of HCl with ice is also important in the heterogeneous chemistry of the upper troposphere[9,10] and polar stratosphere.[11,12] HCl diffusion in ice can affect the reaction kinetics of chlorine activation on ice clouds and influence the ability of ice particles to sequester HCl. HCl diffusion can also control the extent of HCl removal from the gas phase via sedimentation and influence the dechlorination of the polar stratosphere.[13]

HCl diffusion in ice has been investigated using a variety of experimental techniques including infrared LRD depth-profiling,[14,15] microtome sectioning and liquid chromatography,[6,8,16] radioactive tracer methods,[17] scanning electron microscopy (SEM) and X-ray analysis,[18] and attenuated total internal reflection infrared (ATR-IR) spectroscopy.[19] Conflicting HCl diffusion kinetics have been measured with reported HCl diffusion coefficients ranging from $D \sim 10^{-5}$ cm^2/s to $D \sim 10^{-13}$ cm^2/s at $T \sim 185$ K.[2,6,8,14−17,19−23] The various HCl exposure conditions and HCl concentrations, as well as different ice growth conditions, ice morphologies, and spatial resolutions and detection sensitivities may have influenced the HCl diffusion measurements.

The diffusion coefficients determined for HCl and other species in ice are generally much larger than the diffusion coefficients derived from ice core analysis. Polar ice core data reveal clear annual cycles for Cl^- and many species that correspond to migration distances of <1 cm over time periods of ∼10−20 kiloyears.[2] These distances and time intervals imply maximum apparent diffusion coefficients of $D \sim 10^{-12}$ cm^2/s at $T \sim 240$ K. The disparity between the inferences from ice core analysis and the experimental diffusion measurements may be explained, in part, by variable impurity trapping effects. The glacial ice core is a heterogeneous system where many co-adsorbed anion and cation species may interact strongly to impede diffusion. The experimental diffusion rate for species in pure ice may be inherently faster because of the absence of coadsorbates.

Cooperative trapping effects of anions and cations have been proposed to explain the location and movement of several species in Antarctic ice.[2,24,25] Analysis of Dolleman Island, Antarctic ice cores has revealed that near the ice surface, the Na^+ and Mg^{2+} cation peaks are in-phase with a ratio close to the ratio found in seawater because of their common origin from sea salt particles.[2] However, the Na^+ and Mg^{2+} peaks are out-of-phase with the Mg^{2+} feature split into two peaks centered around the Na^+ peak at depths >10 m. Since diffusion would lead only to a broadening of the existing peaks, the formation

* Corresponding Author. Fax: 303-492-5894. E-mail: Steven.George@Colorado.edu.
† Department of Chemistry and Biochemistry.
‡ Current Address. The Aerospace Corporation, Center for Microtechnology, 2350 E. El Segundo Blvd., El Segundo, CA 90245.
§ Department of Chemical Engineering.

10.1021/jp0145309 CCC: $22.00
Published on Web 04/30/2002

of new peaks may be caused by anion trapping (e.g., Cl^-) and salt formation with the Na^+ or Mg^{2+} cation species.[2]

The seasonal trends observed for nitrate in Summit, Greenland polar ice have also been correlated with ion interactions.[26] Simultaneous measurements of the ice acidity and NO_3^- anion concentrations revealed different behavior in acidic and alkaline ice. In acidic ice, the NO_3^- levels remained approximately constant with no observable seasonality. This NO_3^- smoothing was consistent with the ability of NO_3^- to diffuse through the acidic ice layers. In contrast, the NO_3^- concentrations displayed distinct seasonal patterns in alkaline ice. These narrow seasonal peaks indicated reduced NO_3^- anion mobility that was attributed to the interaction of NO_3^- with cations in alkaline ice such as Ca^{2+} and Na^+.[26]

Although anion−cation trapping phenomena have been suggested to explain previous ice core results, there have been no direct experimental observations. To explore anion−cation trapping phenomena in ice, the present study investigated the trapping effect of sodium on HCl hydrate diffusion in ice. Sodium is one of several metal cations detected in glacial ice cores and originates from marine, continental, and terrestrial sources.[7,27] This study is also complemented by previous measurements of HCl and Na diffusion kinetics in pure ice using infrared laser resonant desorption (LRD) depth-profiling techniques.[14,15,28]

II. Experimental Section

A. Laser Resonant Desorption (LRD) Depth-Profiling. A detailed description has been provided earlier for the experimental setup[14,15,28] and rotary Q-switched Er:YAG laser.[15,29] Briefly, the LRD experiments were conducted in an ultrahigh vacuum (UHV) chamber located on a vibrationally isolated optical table. Crystalline ice films were grown on a single-crystal Ru(001) metal substrate. The excellent lattice match between Ru(001) and hexagonal ice promotes the growth of crystalline ice films.[30] The measurements of HCl hydrate diffusion in pure ice and Na-dosed ice were performed using the infrared LRD depth-profiling technique.[14,15,31]

LRD was accomplished using a Er:YAG TEM_{oo} Q-switched laser (LaserSight Technologies, Inc., Model 1-2-3) with an output wavelength of $\lambda = 2.94\ \mu$m and a pulse duration of ~100 ns. A newly designed close-coupled circular diffuse $BaSO_4$ reflector cavity (Shiva Laser Systems, Inc.) was implemented to achieve high laser output energies and enhanced pulse-to-pulse stability.[15,29] The Er:YAG laser radiation resonantly pumps the O−H stretching vibration in the H_2O molecules in the ice lattice.[31] The incident laser energy is rapidly thermalized and induces desorption from the ice film.

In the LRD depth-profiling experiment, a series of Er:YAG laser pulses was used to desorb iteratively thin layer sections of the ice film.[14,15] The incident laser energy was adjusted to achieve the desired probe depth in the ice film. Previous LRD depth-profiling studies have demonstrated that various H_2O desorption depths can be readily obtained by adjusting the Er:YAG laser pulse energy.[15] Laser pulses were incident at an angle of 54° with respect to the surface normal. The focused Er:YAG laser pulse was Gaussian with a beam waist of ~200 μm (fwhm). This focused laser pulse produced elliptical desorption areas with typical dimensions of ~175 μm × ~225 μm.

The desorbed species were mass analyzed with high sensitivity using an Extrel C50 quadrupole mass spectrometer with line-of-sight to the ionizer. Consecutive laser pulses desorbed deeper into the ice bulk. The quadrupole mass spectrometer signals were recorded for each Δx sublayer. These measurements

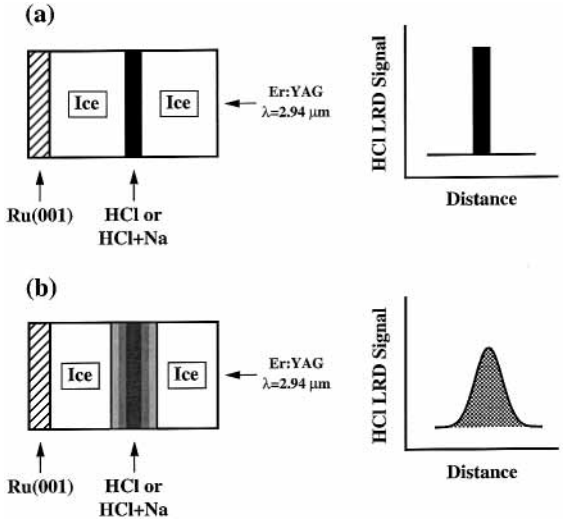

Figure 1. LRD depth-profiling experiment used to measure HCl hydrate diffusion in ice. (a) Er:YAG laser pulses depth-profile the ice sandwich structure and measure the initial HCl concentration profile. (b) After HCl diffusion, a second LRD depth-profile observes the relaxation of the initial HCl concentration profile.

permitted the concentration profile of the diffusing species to be determined versus distance into the ice bulk. The ice film thickness was determined following LRD depth-profile analysis using optical interferometry during isothermal desorption of the ice film.[32]

B. Measurement of HCl Diffusion Using LRD Depth-Profiling. HCl hydrate diffusion measurements in pure ice and Na-dosed ice were conducted by monitoring the HCl concentration versus time using LRD probing as depicted in Figure 1. A laminated ice/HCl/ice or ice/Na−HCl/ice sandwich structure was prepared by initially growing an ice multilayer on the Ru(001) substrate. The H_2O sample (Optima Grade, Fisher Scientific) was purified by several freeze−pump−thaw cycles with liquid nitrogen prior to use. The bottom ice film layers were grown at temperatures ranging from $T = 100$ to 160 K and subsequently annealed to ensure crystallinity.[30]

A localized HCl trihydrate interlayer was formed by condensing HCl vapor (HCl, >99% anhydrous grade, Aldrich Chemical Co., Inc.) on top of this ice multilayer at $T = 140$ K.[14,33] Low temperatures were employed for HCl deposition to avoid HCl desorption or preliminary HCl diffusion. The H_2O LRD signals and calibrated HCl LRD signals were consistent with initial HCl trihydrate interlayers that ranged in thickness from ~0.02 to 0.1 μm.[14] A localized Na/HCl interlayer was created by depositing Na on top of the HCl/H_2O stacked layer using a Na alkali-metal SAES getter source.[28] Typical Na deposition rates were ~1 ML/min. The Na flux and Na concentration were calibrated using temperature-programmed desorption (TPD) analysis.[28] The ice/HCl/ice or ice/Na−HCl/ice sandwich structures were completed by growing an additional ice layer on top of the HCl or Na/HCl adlayers.

The Er:YAG laser was then used to depth-profile into the ice laminate structure and measure the HCl concentration versus time.[14,15,28] Prior to diffusion, the HCl should remain localized in the ice laminate structure and the initial LRD depth-profile at $t = 0$ should resemble the profile depicted in Figure 1a. The temperature of the ice sandwich was then raised to the diffusion temperature for a fixed time interval. Subsequently, the ice sandwich structure was cooled rapidly to terminate further diffusion and a second LRD depth-profile was obtained using the Er:YAG laser. Diffusion of the HCl interlayer species will

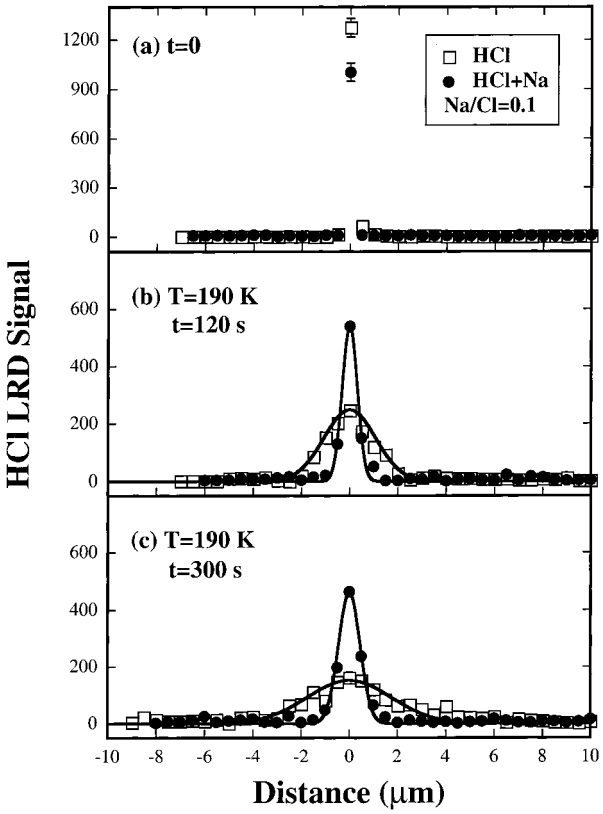

Figure 2. HCl LRD signal versus distance in an ice sandwich multilayer containing either an HCl interlayer (open squares) or a Na/HCl interlayer at a Na/Cl molar ratio of Na/Cl = 0.1 (solid circles) obtained (a) at $t = 0$, (b) after diffusion at $T = 190$ K for $t = 120$ s, and (c) after diffusion at $T = 190$ K for $t = 300$ s.

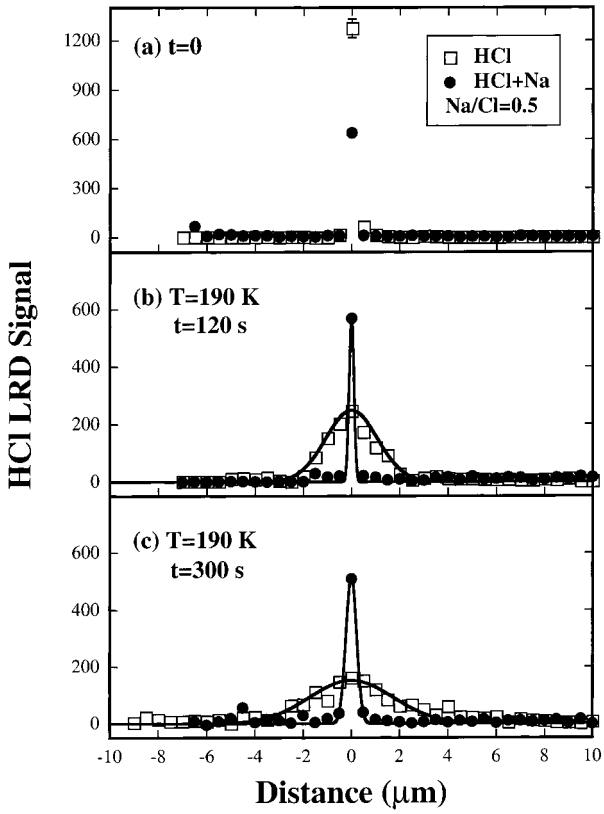

Figure 3. HCl LRD signal versus distance in an ice sandwich multilayer containing either an HCl interlayer (open squares) or a Na/HCl interlayer at a Na/Cl molar ratio of Na/Cl = 0.5 (solid circles) obtained (a) at $t = 0$, (b) after diffusion at $T = 190$ K for $t = 120$ s, and (c) after diffusion at $T = 190$ K for $t = 300$ s.

result in the relaxation of the initial HCl concentration gradient as illustrated in Figure 1b. The HCl concentration profiles measured at successive diffusion times can then be used to derive the HCl diffusion coefficients.[14,15]

III. Results

Figure 2 shows a comparison of the measured HCl LRD signals versus distance in ice sandwich multilayers containing either an HCl interlayer or a Na/HCl interlayer. The HCl LRD diffusion results for the HCl and Na/HCl interlayers are represented by the open squares and solid circles, respectively. The simulations based on Fick's Law are denoted by the solid lines. The Na/Cl molar ratio of the initial Na/HCl interlayer was Na/Cl = 0.1. The incident Er:YAG laser pulse energy was $E = 0.65 \pm 0.02$ mJ and corresponds to an H_2O desorption depth during LRD of 0.53 μm.

The LRD depth-profiling results in Figure 2a at $T = 110$ K show that the HCl hydrate interlayer is initially localized at $t = 0$. The temperature of the ice sandwich structure was then raised to $T = 190$ K for $t = 120$ s with a constant H_2O backing pressure and subsequently cooled rapidly to ~110 K to terminate further HCl diffusion. The HCl LRD signals versus distance into the ice sandwich structure are shown in Figure 2b. LRD results reveal that the HCl concentration gradient in pure ice has relaxed considerably with HCl hydrate diffusion occurring over ~2 μm. The diffusion simulations yield a HCl hydrate diffusion coefficient of $D = 4.8(\pm 1.5) \times 10^{-11}$ cm^2/s.

The HCl hydrate diffusion is very different in the presence of Na. Figure 2b shows the LRD results for an Na/HCl interlayer with an initial molar ratio of Na/Cl = 0.1. These results demonstrate that HCl diffusion is reduced markedly by Na. The HCl concentration profile at $t = 120$ s reveals limited HCl hydrate diffusion of only ~0.5 μm. Diffusion simulations are consistent with a HCl hydrate diffusion coefficient of $D = 4.0(\pm 0.6) \times 10^{-12}$ cm^2/s.

The LRD depth-profiling results obtained after HCl hydrate diffusion at $T = 190$ K for $t = 300$ s are shown in Figure 2c. For the HCl interlayer in pure ice, the HCl concentration gradient has relaxed further with HCl migration occurring over lengths of ~4 μm. Diffusion simulations yield a HCl hydrate diffusion coefficient of $D = 5.1(\pm 1.6) \times 10^{-11}$ cm^2/s. In comparison, only small HCl diffusion distances of ~0.5−1.0 μm and a HCl hydrate diffusion coefficient of $D = 3.3(\pm 0.5) \times 10^{-12}$ cm^2/s are observed for the Na/HCl interlayer. HCl hydrate mobility for an initial interlayer molar ratio of Na/Cl = 0.1 is a factor of 13 ± 2 smaller than HCl hydrate mobility in pure ice.

Figure 3 compares HCl LRD signals versus distance in ice sandwich multilayers containing either an HCl interlayer or a Na/HCl interlayer at a higher molar ratio of Na/Cl = 0.5. The incident Er:YAG laser pulse energy was $E = 0.60 \pm 0.01$ mJ and corresponds to an H_2O desorption depth during LRD of 0.48 μm. Figure 3a shows that the HCl interlayer is initially well localized at $t = 0$. Figures 3b and 3c reveal that HCl hydrate diffusion at an initial interlayer molar ratio of Na/Cl = 0.5 was not observed after diffusion times of $t = 120$ s and $t = 300$ s at $T = 190$ K. Since the HCl diffusion lengths do not exceed the H_2O desorption depth of ~0.5 μm, the simulations yield an upper limit to the HCl hydrate diffusion coefficient of $D \leq 9.0 \times 10^{-13}$ cm^2/s. These LRD results demonstrate that HCl hydrate diffusion at an initial molar ratio of Na/Cl = 0.5 is decreased by a factor of ≥57 compared with HCl hydrate diffusion in pure ice.

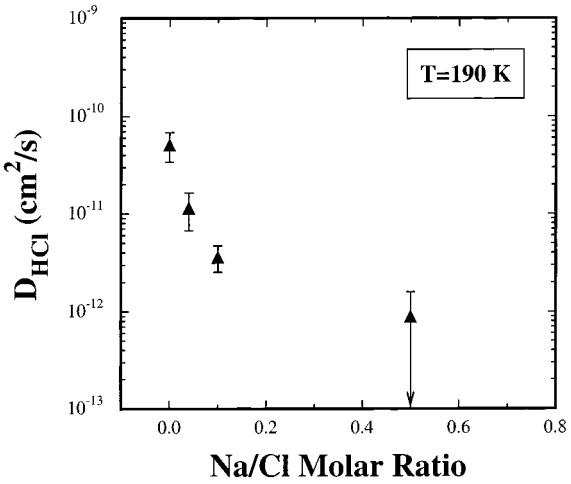

Figure 4. HCl hydrate diffusion coefficient at 190 K measured in ice sandwich multilayers using LRD depth-profiling versus Na/Cl molar ratio of the initial Na/HCl interlayer.

Figure 4 shows the measured HCl hydrate diffusion coefficient versus the initial interlayer Na/Cl molar ratio at $T = 190$ K. The HCl hydrate diffusion coefficient in pure ice is $D = 5.1(\pm 1.7) \times 10^{-11}$ cm^2/s at $T = 190$ K. The HCl hydrate diffusion coefficients in the presence of sodium vary from $D = 1.2(\pm 0.5) \times 10^{-11}$ cm^2/s to $D \leq 9.0 \times 10^{-13}$ cm^2/s at interlayer molar ratios of Na/Cl = 0.04 to Na/Cl = 0.5, respectively. The HCl hydrate diffusion rate in ice is reduced significantly by sodium. Interlayer molar ratios higher than Na/Cl = 0.5 were not employed because the HCl migration lengths were less than the H_2O desorption depth during LRD of $\sim$0.5 μm.

IV. Discussion

The HCl molecules were contained in the ice/HCl/ice sandwich structure with a local H_2O:HCl stoichiometry of 3:1. This H_2O:HCl ratio corresponds to a HCl trihydrate phase with a thickness of $\sim$0.02 μm and $\sim$0.1 μm for Figures 2 and 3, respectively.[33] HCl diffusion from this trihydrate phase involves the migration and dilution of various HCl hydrate phases through the ice lattice. Numerous studies exist concerning the formation and identification of amorphous and crystalline HCl hydrates in ice.[22,33−37] Amorphous HCl−ice hydrate thin films with various H_2O:HCl stoichiometries have been observed using infrared (IR) spectroscopy.[22,34,35] IR spectroscopy and laser-induced thermal desorption (LITD) techniques have also been utilized to assign the various mono-, di-, tri-, tetra-, and hexahydrate phases of crystalline HCl hydrates in ice over the temperature range from $T = 85$ to 215 K.[22,33−37] Numerous studies have also been conducted to define the various hydrates on the HCl/ice phase diagram.[8,38,39]

HCl dissociates in ice to form H_3O^+ and Cl^-. The H_3O^+ hydronium ion is observed in the infrared spectrum of ice exposed to HCl.[19] Theoretical calculations confirm the facile dissociation and ionization of HCl on ice surfaces.[40] The high HCl concentrations observed on ice surfaces also must be explained by HCl dissociation.[41] The low calculated adsorption energy of $\sim$5−7 kcal/mol for molecular HCl on ice surfaces is insufficient to rationalize HCl adsorption on ice and HCl uptake into ice.[41]

HCl hydrate diffusion in ice is postulated to occur by H_3O^+ and Cl^- migration into vacancies in the ice lattice.[14] The movement of Cl^- anions may be impeded by cations. The coadsorbed Na in the H_2O/Na−HCl/H_2O sandwich structures is believed to correspond to sodium in its ionized cationic form, Na^+. Sodium could ionize in ice by forming a solvated electron via $Na + nH_2O \rightarrow Na^+ + e^-(H_2O)_n$. This ionization process is supported by numerous experimental[42−47] and theoretical[48,49] studies. Sodium could also undergo ionization by reacting with H_2O to produce H_2: $Na + H_2O \rightarrow Na^+ + OH^- + {}^1/_2H_2$.[43,50]

We could not determine the reaction that converts sodium atoms into sodium ions. H_2 evolution was not observed during Na exposure onto the ice multilayer. However, the Na fluxes were very low and there is a finite H_2 background pressure in our UHV chamber. An electron current to the Ru(001) substrate may also be present during solvated electron formation. We did not attempt to measure this possible electron current. Our main supporting evidence for Na^+ in ice is provided by the LRD measurements that detect Na^+ with the ionizer of the mass spectrometer either on or off.[28] This observation is consistent with direct Na^+ desorption from Na/ice.

The LRD results in Figures 2−4 demonstrate that sodium can dramatically alter HCl hydrate diffusion in ice. This study represents the first direct experimental investigation of trapping in ice. The trapping effect of Na is attributed to direct anion−cation interactions and an immobile NaCl salt in ice. Longer ranged electrostatic interactions between the Na^+ and Cl^- hydrated ions may also contribute to the observed trapping behavior. An alternative possibility is that NaCl salt has very little solubility in ice. The majority of the NaCl salt species would then be forced to remain at the interface of the ice sandwich structure because only a limited concentration is soluble in the ice bulk. Whatever the origin of the immobile NaCl salt, similar trapping processes may influence mobility in ice and alter the historical record of Earth's atmosphere contained in glacial and polar ice cores.

The trapping effect of Na on HCl hydrate diffusion in ice may not be directly relevant to HCl diffusion in ice cores. HCl LRD signals near the center of the concentration profiles in Figures 2 and 3 correspond to HCl levels of $\sim(5-10) \times 10^8$ molecules/μm^3 or $\sim$0.01−0.02 HCl mole fraction. The HCl concentrations in the low intensity wings of the concentration profiles are typically $\leq$10% of the maximum HCl concentrations. In comparison, a variety of laboratory studies have measured HCl impurity solubilities in ice ranging from 1.3×10^{-7} to 1.8×10^{-4} mole fraction ($\sim$0.3 to 360 ppm by mass) over a temperature range from $T = 190-273$ K.[6,8,16−18,51−54] A recent comprehensive examination measured equilibrium HCl mole fractions that varied from 1.24×10^{-6} to 12.36×10^{-6} (2.48−24.72 ppm by mass) over the temperature range from 238 to 265 K.[8]

The HCl concentrations measured in these LRD studies of HCl hydrate diffusion are much larger than the HCl impurity solubilities in ice under atmospheric conditions or HCl concentrations in ice cores.[55,56] The HCl/ice phase diagram reveals that the HCl hydrates examined in these LRD experiments can be formed only at lower temperatures or higher HCl partial pressures than are typical under atmospheric conditions.[38] The HCl detection limit for the LRD depth-profiling technique coupled with quadrupole mass spectrometry is $\sim 2 \times 10^{-6}$ HCl mole fraction or $\sim$4 ppm HCl by mass.[14] The LRD depth-profiling studies have the sensitivity to detect HCl impurity concentrations in ice only at the maximum solubilities of 10−25 ppm HCl by mass.

The Na detection limits for LRD coupled with quadrupole mass spectrometry is 1×10^{-8} Na mole fraction or $\sim$10 ppb Na by mass.[28] This sensitivity is adequate to detect Na in ice core samples. Na levels measured in natural Antarctic ice

samples range from ~8 to 170 ng Na/g or ~0.01 to 0.20 ppm Na by mass for the Holocene and last glacial maximum periods.[56,57] For the Arctic polar region, Na concentrations vary from ~1 to 100 ng Na/g or $\sim 1 \times 10^{-3}$ to 0.13 ppm Na by mass.[27] The HCl/Na ice sandwich experiments utilized much higher Na concentrations to be comparable with the HCl concentrations. The center of the concentration profiles in Figures 2 and 3 correspond to Na concentrations that range from $\sim(1.5 \text{ to } 8) \times 10^7$ molecules/μm^3 or $\sim(0.6 \text{ to } 3) \times 10^{-3}$ Na mole fraction. These Na concentrations allowed the Na/Cl molar ratio to be varied from Na/Cl = 0.04 to Na/Cl = 0.5.

Although the HCl concentrations in these LRD investigations are much higher than HCl solubility limits in ice under atmospheric conditions, the trapping effect by sodium is dramatic. The proposed anion−cation trapping interaction between Cl^- and Na^+ may also occur at much lower HCl concentrations in ice core samples. These trapping interactions may alter the Cl^- distributions and change the interpretation of ice core analysis. As discussed earlier, anion−cation trapping may explain the location and movement of Na^+ and Mg^{2+} in Dolleman Island, Antarctic ice cores.[2] Likewise, anion−cation trapping in alkaline ice may explain the enhanced NO_3^- mobility in acidic ice.[26]

Other examples of anion−cation trapping have also been suggested to explain ice core signatures. Analysis of ice cores from Dolleman Island and Berkner Island in the Antarctic Peninsula has revealed that the methanesulfonate anion (MSA^-) has migrated from the summer snow layer where MSA^- was initially deposited to the winter snow layer.[24,25] The translocation of MSA^- does not result in a smoothing of the MSA^- concentration profiles that would normally be associated with a diffusion process. The MSA^- layers remain well defined with the winter peaks becoming sharper versus ice core depth.[24,25] The proposed mechanism of MSA^- movement and localization involves diffusion of MSA^- into the winterlayer where the MSA^- anion is trapped via insoluble salt formation with a prevalent cation species.[24]

V. Conclusions

The results of this LRD depth-profiling study demonstrate that the diffusion of HCl hydrates in ice can be reduced dramatically by sodium. Compared with HCl hydrate diffusion in pure ice, the HCl hydrate diffusion coefficients at 190 K are reduced by factors of 4 ± 1 to ≥ 57 in ice containing initial interlayer molar ratios of Na/Cl = 0.04 to Na/Cl = 0.5, respectively. This reduction is attributed to the trapping of Cl^- anions by Na^+ cations to form a NaCl salt in the ice. These LRD results support the hypothesis that anion−cation trapping processes may account for the localization of various anions and cations in polar ice.

These LRD measurements may not be directly related to HCl diffusion in ice core samples. The HCl concentrations in the HCl hydrates and the variable Na trapping concentrations are higher than typical HCl and Na impurity levels in ice core samples. However, these LRD measurements do provide the first direct experimental verification for significant anion−cation trapping effects in ice. These trapping interactions may explain the variation between different diffusion measurements and the apparent contradiction between experimental diffusion measurements in pure ice and inferences about diffusion in ice from ice core analysis.

Acknowledgment. The authors gratefully acknowledge the financial support of the National Science Foundation under Grant CHE-9905812.

References and Notes

(1) Hobbs, P. V. *Ice Physics*; Clarendon Press: Oxford, 1974.
(2) Wolff, E. W.; Bales, R. C. *Chemical Exchange Between the Atmosphere and Polar Snow*; Springer-Verlag: Berlin, 1996.
(3) Petrenko, V. F.; Whitworth, R. W. *Physics of Ice*; Oxford University Press: New York, 1999.
(4) Petit, J. R.; Jouzel, J.; Raynaud, D.; Barkov, N. I.; Barnola, J.-M.; Basile, I.; Bender, M.; Chappellaz, J.; Davis, M.; Delaygue, G.; Delmotte, M.; Kotlyakov, V. M.; Kegrand, M.; Lipenkov, V. Y.; Lorius, C.; Pepin, L.; Ritz, C.; Saltzman, E.; Stievenard, M. *Nature* **1999**, *399*, 429.
(5) Delmas, R. J.; Legrand, M. Long-Term Changes in the Concentrations of Major Chemical Compounds (Soluble and Insoluble) Along Deep Ice Cores. In *The Environmental Record in Glaciers and Ice Sheets Dahlem Workshop Report*; Oeschger, H., Langway, C. C., Eds.; Wiley and Sons: Chichester, 1989.
(6) Domine, F.; Thibert, E.; Silvente, E.; Legrand, M.; Jaffrezo, J.-L. *J. Atmos. Chem.* **1995**, *21*, 165.
(7) Legrand, M.; Mayewski, P. *Rev. Geophys.* **1997**, *35*, 219.
(8) Thibert, E.; Domine, F. *J. Phys. Chem. B* **1997**, *101*, 3554.
(9) Borrmann, S.; Solomon, S.; Dye, J. E.; Luo, B. *Geophys. Res. Lett.* **1996**, *23*, 2133.
(10) Zondlo, M. A.; Barone, S. B.; Tolbert, M. A. *Geophys. Res. Lett.* **1997**, *24*, 1391.
(11) Solomon, S. *Rev. Geophys.* **1988**, *26*, 131.
(12) Hanson, D. R.; Ravishankara, A. R. *J. Geophys. Res.* **1991**, *96*, 5081.
(13) Domine, F.; Thibert, E.; Van Landeghem, F.; Silvente, E.; Wagnon, P. *Geophys. Res. Lett.* **1994**, *21*, 601.
(14) Livingston, F. E.; George, S. M. *J. Phys. Chem. A* **2001**, *105*, 5155.
(15) Livingston, F. E.; Smith, J. A.; George, S. M. *Anal. Chem.* **2000**, *72*, 5590.
(16) Domine, F.; Thibert, E. *Geophys. Res. Lett.* **1996**, *23*, 3627.
(17) Krishnan, P. N.; Salomon, R. E. *J. Phys. Chem.* **1969**, *73*, 2680.
(18) Wolff, E. W.; Mulvaney, R.; Oates, K. *Geophys. Res. Lett.* **1989**, *16*, 487.
(19) Horn, A. B.; Sully, J. *J. Chem. Soc., Faraday Trans.* **1997**, *93*, 2741.
(20) Barnaal, D.; Slotfeldt-Ellingsen, D. *J. Phys. Chem.* **1983**, *87*, 4321.
(21) Molina, M. J.; Tso, T. L.; Molina, L. T.; Wang, F. C. Y. *Science* **1987**, *238*, 1253.
(22) Koehler, B. G.; McNeill, L. S.; Middlebrook, A. M.; Tolbert, M. A. *J. Geophys. Res.* **1993**, *98*, 10563.
(23) Chu, L. T.; Leu, M.-T.; Keyser, L. F. *J. Phys. Chem.* **1993**, *97*, 7779.
(24) Pasteur, E. C.; Mulvaney, R. *J. Geophys. Res.* **2000**, *105*, 11.
(25) Mulvaney, R.; Pasteur, E. C.; Peel, D. A.; Saltzman, S.; Whung, P.-Y. *Tellus* **1992**, *44B*, 295.
(26) Thibert, E.; Domine, F. *J. Phys. Chem. B* **1998**, *102*, 4432.
(27) De Angelis, M.; Steffensen, J. P.; Legrand, M.; Clausen, H.; Hammer, C. *J. Geophys. Res.* **1997**, *102*, 26.
(28) Livingston, F. E.; George, S. M. *J. Phys. Chem. B* **2001**, submitted.
(29) Livingston, F. E.; George, S. M.; Shori, R. K. *Rev. Sci. Instrum.* **2002**, in press.
(30) Brown, D. E.; George, S. M. *J. Phys. Chem.* **1996**, *100*, 15460.
(31) Krasnopoler, A.; George, S. M. *J. Phys. Chem. B* **1998**, *102*, 788.
(32) Haynes, D. R.; Tro, N. J.; George, S. M. *J. Phys. Chem.* **1992**, *96*, 8502.
(33) Foster, K. L.; Tolbert, M. A.; George, S. M. *J. Phys. Chem.* **1997**, *101*, 4979.
(34) Delzeit, L.; Rowland, B.; Devlin, J. P. *J. Phys. Chem.* **1993**, *97*, 10312.
(35) Ritzhaupt, G.; Devlin, J. P. *J. Phys. Chem.* **1991**, *95*, 90.
(36) Abbatt, J. P.; Beyer, K. D.; Fucaloro, A. F.; McMahon, J. R.; Woolridge, P. J.; Zhang, R.; Molina, M. J. *J. Geophys. Res.* **1992**, *97*, 15819.
(37) Gilbert, A. S.; Sheppard, N. *J. Chem. Soc., Faraday Trans. 2* **1973**, *69*, 1628.
(38) Molina, M. J. The Probable Role of Stratospheric "Ice" Clouds: Heterogeneous Chemistry of the "Ozone Hole". In *The Chemistry of the Atmosphere: Its Impact on Global Change*; Calvert, J. G., Ed.; Blackwell Scientific: Boston, MA, 1994.
(39) Wooldridge, P. J.; Zhang, R.; Molina, M. J. *J. Geophys. Res.* **1995**, *100*, 1389.
(40) Gertner, B. J.; Hynes, J. T. *Science* **1996**, *271*, 1563.
(41) Kroes, G.-J.; Clary, D. C. *J. Phys. Chem. A* **1992**, *96*, 7079.
(42) Mayer, T.; Jaegermann, W. *J. Phys. Chem. B* **2000**, *104*, 5945.
(43) Gunster, J.; Krischok, S.; Stultz, J.; Goodman, D. W. *J. Phys. Chem. B* **2000**, *104*, 7977.
(44) Buck, U.; Steinbach, C. *J. Phys. Chem. A* **1998**, *102*, 7333.
(45) Bewig, L.; Buck, U.; Rakowsky, S.; Reymann, M.; Steinbach, C. *J. Phys. Chem. A* **1998**, *102*, 1124.
(46) Martin, T. P. *Clusters of Atoms and Molecules I*; Springer: Berlin, 1995.

(47) Goerke, A.; Leipelt, G.; Palm, H.; Schulz, C. P.; Hertel, I. V. *Z. Phys. D* **1995**, *32*, 311.
(48) Barnett, R. N.; Landman, U. *Phys. Rev. Lett.* **1993**, *70*, 1775.
(49) Kim, J.; Lee, S.; Cho, S. J.; Mhin, B. J.; Kim, K. S. *J. Chem. Phys.* **1995**, *102*, 839.
(50) Doering, D. L.; Semancik, S.; Madey, T. E. *Surf. Sci.* **1983**, *133*, 49.
(51) Hanson, M.; Mauersberger, K. *Geophys. Res. Lett.* **1988**, *15*, 1507.
(52) Hanson, D. R.; Mauersberger, K. *J. Phys. Chem.* **1990**, *94*, 4700.
(53) Gross, G. W.; Wong, P. W.; Humes, K. J. *J. Chem. Phys.* **1977**, *67*, 5264.
(54) Seidensticker, R. G. *J. Chem. Phys.* **1972**, *56*, 2853.
(55) Legrand, M. R.; Delmas, R. J. *J. Geophys. Res.* **1988**, *93*, 7153.
(56) Legrand, M. R.; Delmas, R. J. *Atmos. Environ.* **1984**, *18*, 1867.
(57) De Angelis, M.; Legrand, M.; Petit, J. R.; Barkov, N. I.; Korotkevitch, Y. S.; Kotlyakov, V. M. *J. Atmos. Chem.* **1984**, *1*, 215.